ACS central science

http://pubs.acs.org/journal/acscii

Research Article

Single Metal Site and Versatile Transfer Channel Merged into Covalent Organic Frameworks Facilitate High-Performance Li-CO_2 Batteries

Yu Zhang,[⊥] Rong-Lin Zhong,[⊥] Meng Lu,[⊥] Jian-Hui Wang, Cheng Jiang, Guang-Kuo Gao, Long-Zhang Dong, Yifa Chen, Shun-Li Li, and Ya-Qian Lan*

Cite This: *ACS Cent. Sci.* 2021, 7, 175−182

Read Online

ABSTRACT: The sluggish kinetics and unclear mechanism have significantly hindered the development of Li-CO_2 batteries. Here, a Li-CO_2 battery cathode catalyst based on a porphyrin-based covalent organic framework (TTCOF-Mn) with single metal sites is reported to reveal intrinsic catalytic sites of aprotic CO_2 conversion from the molecular level. The battery with TTCOF-Mn exhibits a low overpotential of 1.07 V at 100 mA/g as well as excellent stability at 300 mA/g, which is one of the best Li-CO_2 battery cathode catalysts to date. The unique features of TTCOF-Mn including uniform single-Mn(II)-sites, fast Li^+ transfer pathways, and high electron transfer efficiency contribute to effective CO_2 reduction and Li_2CO_3 decomposition in the Li-CO_2 system. Density functional theory calculations reveal that different metalloporphyrin sites lead to different reaction pathways. The single-Mn(II) sites in TTCOF-Mn can activate CO_2 and achieve an efficient four-electron CO_2 conversion pathway. It is the first example to reveal the catalytic active sites and clear reaction pathways in aprotic Li-CO_2 batteries.

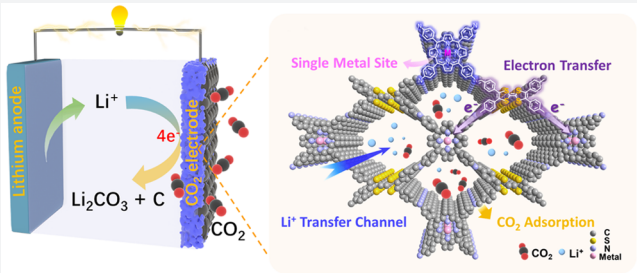

■ INTRODUCTION

Aprotic lithium−carbon dioxide (Li-CO_2) batteries based on the electrochemical reactions of CO_2 reduction and evolution provide an effective CO_2 fixation strategy as well as a novel energy storage technology for multifarious applications and thus have attracted increasing attention and have been investigated worldwide in recent years.[1,2] The multielectron battery reactions endow the Li-CO_2 battery with a theoretical energy density as high as 1876 Wh/kg, which is far more than that of Li-ion batteries, making it a promising alternative power supply in some specific circumstances, like submarines operation or Mars exploration.[3] Plenty of nanomaterials that have performed outstandingly in Li-O_2 batteries or other metal-air batteries, such as carbon-based materials,[4−6] transition metal oxides,[7,8] and some noble metals,[9,10] have been introduced and utilized in Li-CO_2 batteries and have made significant progress in seeking effective cathode catalysts. Yet, as a result of the inert CO_2 molecules and stable discharge products (usually Li_2CO_3), the sluggish kinetics of CO_2 reduction/evolution involving CO_2 activation and decomposition of the insulative discharge product has led to disappointing reversibility and poor cycling, which largely restrict the appreciable application of the Li-CO_2 battery.[11]

Multidimensional efforts have been devoted to addressing the issues as well as exploring the electrochemical mechanism of Li-CO_2 batteries by designing effective cathode catalysts, such as reducing the overpotential during charging by prompting the decomposition of the discharge products via Ru-based materials[12] and combining ion liquid additives in the electrolyte with an MoS_2 cathode to help form a conductive carbon discharge product.[13] Unfortunately, as a result of the complicated multielectron discharge−charge processes that involve solid−liquid−gas three-phase reactions, the electrochemical pathways and catalytic mechanism are still understood in a limited way. There is still an essential demand to find robust cathode catalysts with well-defined structures to reveal active sites of CO_2 reduction and evolution from the molecular level, and more importantly, to provide some instructions to the rational design of further Li-CO_2 battery cathode catalysts. On the basis of the bottlenecks of the Li-CO_2 battery and advantages of the currently reported cathode catalysts, as shown in Scheme 1, it could be concluded that the design of cathode catalysts should obey the follow principles: (i) having good CO_2 capture capability, (ii) possessing

Received: October 14, 2020
Published: December 29, 2020

Scheme 1. Illustration of the Advantages of TTCOF-M Acting as Li-CO_2 Battery Cathode Catalysts

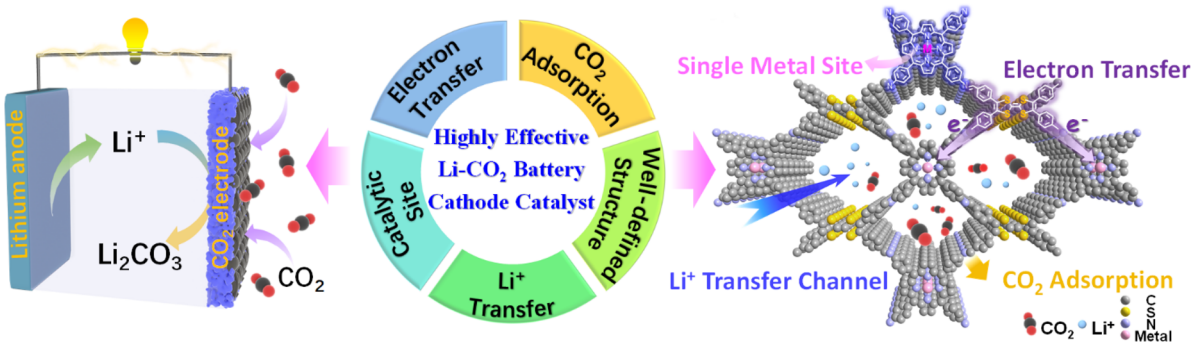

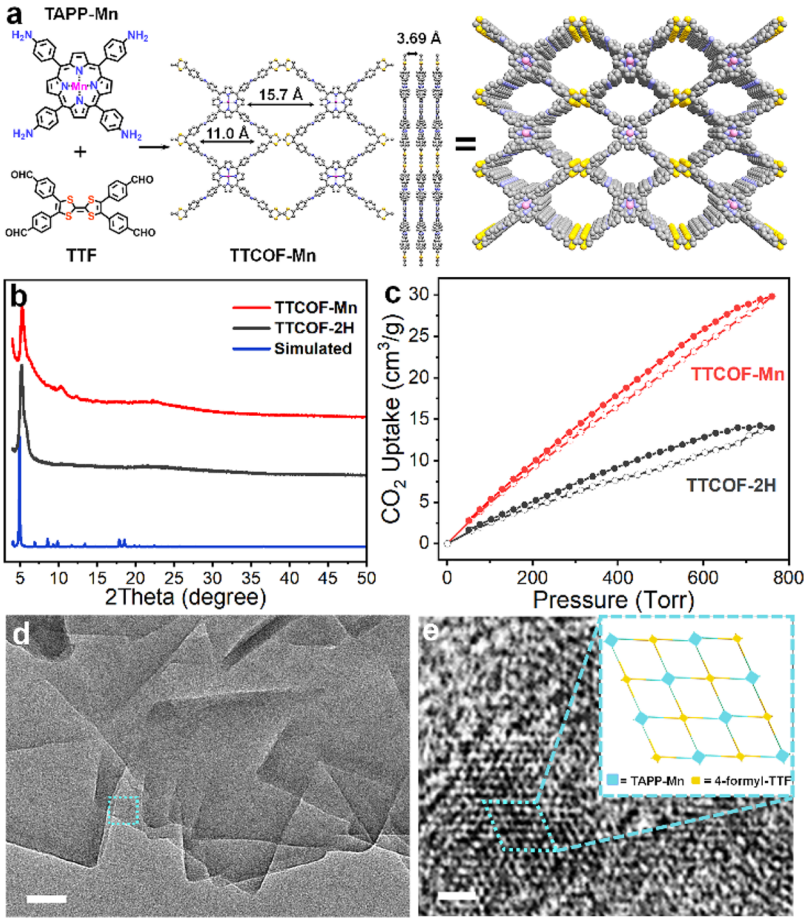

Figure 1. Structural and morphological characterizations. (a) Synthesis route and building blocks of TTCOF-Mn and its top and side viewed structure. (b) Simulated (blue) and experimental PXRD patterns of TTCOF-Mn (red) and TTCOF-2H (black). (c) CO_2 adsorption−desorption isotherms of TTCOF-Mn (red) and TTCOF-2H (black). (d) TEM image (scale bar: 50 nm) and (e) HRTEM image (scale bar: 5 nm) of TTCOF-Mn; the inset is the AA-stacking mode of the 2D TTCOF-Mn structure.

uniform and well-defined catalytic sites for CO_2 reduction/evolution, (iii) offering fast Li ion transfer pathways, (iv) ensuring efficient electron transfer, and (v) presenting a well-defined structure for precise mechanism exploration.

Single-site catalysts (SSCs) featuring well-defined, isolated, and atomically dispersed uniform single-metal active sites have become attractive candidates for achieving controllable catalysis with precise catalytic centers.[14] Covalent organic frameworks (COFs), especially those that contain metalloporphyrin moieties, have provided a promising platform to construct single-site catalysts due to the spatially separated and unsaturated coordinated single-metal sites.[15] The evenly distributed atomically precise single metalloporphyrin sites have been reported to be active for CO_2 reduction in electro-/photocatalysis.[16−19] Therefore, it is timely to investigate the catalytic mechanism of aprotic CO_2 conversion on metalloporphyrin sites. In addition, as a kind of crystalline carbon-based material, COFs offering structural diversity with tunable porosity, high surface area, and controllable skeletons[20,21] have been applied in the gas storage/separation and show excellent CO_2 capture ability,[22−24] which would be beneficial to the mass transport and ion migration during battery reactions. Indeed, it has been reported that the addition of a hydrazine-linked COF (Tf-DHzOPr COF) can enhance CO_2 adsorption

https://dx.doi.org/10.1021/acscentsci.0c01390
ACS Cent. Sci. 2021, 7, 175−182

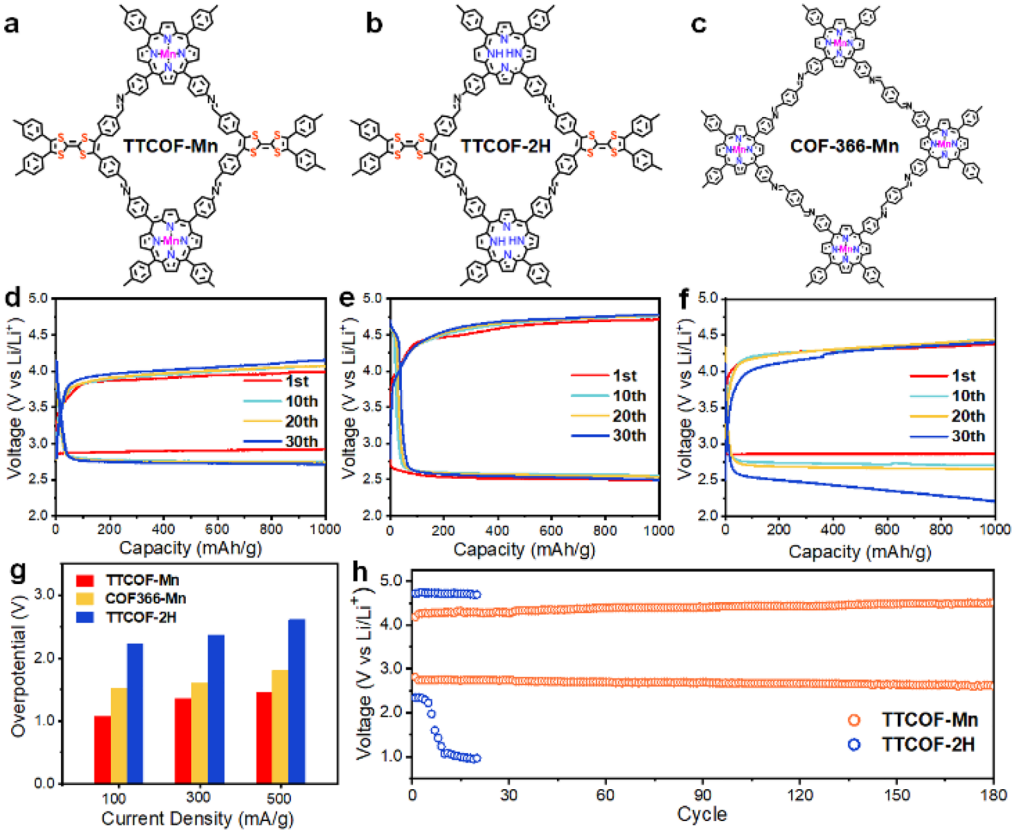

Figure 2. Electrochemical performance of the Li-CO_2 battery using different COF cathode catalysts. (a−c) Molecular structures of TTCOF-Mn, TTCOF-2H, and COF-366-Mn, respectively. Charging/discharging curves of different COF cathode catalysts with the limited capacity of 1000 mAh/g at 100 mA/g: (d) TTCOF-Mn, (e) TTCOF-2H, and (f) COF-366-Mn. (g) Overpotentials of different COF cathode catalysts under current densities of 100 mA/g, 300 mA/g, and 500 mA/g. (h) Long-term cycling of the TTCOF-Mn cathode catalyst and TTCOF-2H cathode catalyst at a current density of 300 mA/g.

and facilitate the Li^+ transfer of Ru/CNTs cathode catalysts and thus lead to improved rate performance of Li-CO_2 battery.[25] Furthermore, it is notable that the combination of an electron-donating ligand, like tetrathiafulvalene (TTF), with the electron-accepting metalloporphyrin would enhance the electron efficiency and accelerate the intermolecular charge-electron transfer pathway to allow CO_2 catalytic activation.[26−28] Thus, the introduction of a single-site catalyst based on COF (TTCOF-M) obtained by TTF and metalloporphyrin to explore the intrinsic catalytic sites and specific reaction pathways during the discharging−charging process in aprotic Li-CO_2 batteries is promising and crucial.

Herein, a porphyrin-based covalent organic framework (TTCOF-Mn) synthesized via the covalent connection between the electron-donating TTF ligand and catalytically active tetrakis(4-aminophenyl)-porphinato manganese(II) (TAPP-Mn) has been designed as an efficient cathode catalyst according to the demand of a high-performance Li-CO_2 battery. The as-designed TTCOF-Mn cathode catalyst with abundant single-metal catalytic sites and uniform microporous channels exhibits a low terminal potential gap of 1.07 V between the discharge and charge potential at a current density of 100 mA/g as well as excellent performance of running for 180 cycles at a current density of 300 mA/g. It is one of the best Li-CO_2 battery cathode catalysts ever reported. The Mn-TAPP single-site in TTCOF-Mn has been proven to be the active site for boosting CO_2 reduction in aprotic Li-CO_2 batteries. Moreover, both the electron-donating properties of TTF and the uniform micropore channels ensure the effective electron transfer, high CO_2 adsorption, and rapid Li ion transport, and simultaneously contribute to the efficient discharge−charge processes on the TTCOF-Mn cathode catalyst. In addition, because of the well-defined structure of COF, the optimal reaction pathways have been proposed on the basis of density functional theory (DFT) calculations, which reveals that the Mn-TAPP sites have a strong adsorption on the CO_2 molecule and can achieve an effective four-electron aprotic CO_2 conversion process. This is the very first time to reveal the catalytic active sites and clear reaction pathways in an aprotic Li-CO_2 system based on the combination between electrochemical results and theoretical calculation of a crystalline catalyst with a precise structure.

■ RESULTS AND DISCUSSION

TTCOF-M formed by covalently connecting between TTF and TAPP-M have been designed in this work to construct effective single-site cathode catalysts for high-performance Li-CO_2 batteries. We synthesized different TTCOF-M (M = 2H, Mn, Co, Ni, Cu) to explore their catalytic activity serving as CO_2-cathode catalysts. TTCOF-Mn is taken as an example in the following discussion. The TTCOF-Mn was synthesized by a modified solvothermal method via Schiff-base condensation between TAPP-Mn and TTF in the presence of aqueous acetic acid (Figure 1a).[18,19] According to the refined crystal structure in the AA stacking mode, the TTCOF-Mn possesses dual microporous channels with pore sizes of 1.10 and 1.57 nm,

https://dx.doi.org/10.1021/acscentsci.0c01390
ACS Cent. Sci. 2021, 7, 175−182

respectively. And the distance between the COF-stacking layers is 3.69 Å theoretically. As shown in Figure 1b, the powder X-ray diffraction (PXRD) pattern confirms that the as-synthesized TTCOF-Mn is crystalline, which is similar to that of previously reported TTCOF-2H. The strong diffraction peaks centered at 5.26° in the TTCOF-Mn PXRD pattern are attributed to the (110) faces.[18] The chemical structure of TTCOF-Mn is also verified by Fourier transform infrared (FT-IR) spectra shown in Figure S1 in which similar peaks at around 1622 cm^{-1} in TTCOF-2H and TTCOF-Mn appear, indicating the existence of a C═N bond in the structures due to the successful covalent connection between TTF and TAPP-Mn.

The structural porosity of TTCOF-Mn was further characterized by gas sorption measurements. Nitrogen adsorption−desorption curves display a typical reversible isotherm representing a characteristic of microporous materials for TTCOF-Mn (Figure S2). The prepared TTCOF-Mn exhibits a Brunauer−Emmett−Teller (BET) surface area of 760.5 m^2/g with a total pore volume of 0.8 cm^3/g. The pore size distribution suggests two main pore widths of 0.88 and 1.30 nm, which are a little smaller but still reasonable compared to the theoretical values. CO_2 adsorption experiments are carried out at 298 K to examine the CO_2 capture ability of the synthesized COFs (Figure 1c). The TTCOF-Mn and TTCOF-2H shows a CO_2 uptake capacity of 29.8 cm^3/g and 14.0 cm^3/g, respectively. The higher CO_2 adsorption of TTCOF-Mn than that of TTCOF-2H implies that the coordination of Mn atom in the porphyrin center promotes the adsorption capacity of CO_2.

The morphology of the synthesized TTCOF-Mn was characterized by transmission electron microscopy (TEM). Figure 1d shows the typical TEM image of TTCOF-Mn, demonstrating square-like nanosheets with a width of 300−500 nm. The high-resolution transmission electron microscopy (HRTEM) image presented in Figure 1e shows the ordered hexagonal pore structural arrangement, consistent with the AA-stacking mode of the 2D TTCOF-Mn structure (inset in Figure 1e). In addition, the TEM energy-dispersive X-ray spectroscopy (TEM-EDX) analysis indicates the homogeneous distribution of C, S, N, and Mn in TTCOF-Mn nanocrystals (Figure S3). The state of Mn species is bivalent in TTCOF-Mn as revealed by XPS shown in Figure S4. The specific contents of Mn element in TTCOF-Mn is 4.11 wt %, determined by ICP-AES (Table S1).

In order to screen out a metalloporphyrin center that is catalytically active toward the Li-CO_2 system, the initial battery performance evaluation of different single-site TTCOF-M (M = Mn, Co, Ni, Cu) cathode catalysts was conducted at first. Figure S10 shows the discharge−charge curves of TTCOF-M cathodes cycled at a constant current density of 100 mA/g with a fixed capacity of 1000 mAh/g, among which the TTCOF-Mn cathode shows better catalytic activity with the highest discharged potential and lowest charged potential compared to the other TTCOF-M cathodes. To investigate the role of metalloporphyrin and firmly verify the catalytic center of the Li-CO_2 system, the electrochemical performance of TTCOF-Mn and TTCOF-2H was compared. As displayed in Figure 2a,b, TTCOF-2H is in the same series with TTCOF-Mn and has a similar structure without a metal atom in the porphyrin center. As shown in Figure 2e, when galvanostatically cycled at 100 mA/g, the TTCOF-2H cathode is discharged at 2.49 V and correspondingly charged at 4.71 V of the first cycle, demonstrating that the TTCOF without the center metal-sites hardly exhibits Li-CO_2 battery activity. Meanwhile, the TTCOF-Mn cathode is discharged at 2.92 V and recharged at 3.99 V of the first cycle, showing a 0.43 V increment and 0.72 V decrease in contrast with the discharge and recharge potential of TTCOF-2H, respectively. In addition, the cyclic voltammetry (CV) curves (Figure S11) disclose that TTCOF-Mn shows a higher cathodic and anodic current and more apparent redox peaks, which further affirms a higher catalytic activity for Li-CO_2 batteries, compared with TTCOF-2H. Preliminarily, it could be speculated that the single-metal porphyrin-Mn site embedded in TTCOF-Mn is the catalytic active center in the Li-CO_2 system.

COF-366-Mn built up by TAPP-Mn and 1,4-benzenedicarboxaldehyde (BDA) (Figure 2c) was synthesized to reveal the role of TTF moieties in TTCOF-Mn cathodes. COF-366-Mn was synthesized by the previously reported method, and the related structure and morphology characterizations are given in Figures S6−S8.[29] Notably, COF-366-Mn shows a charge terminal potential of 4.37 V and also a relatively high discharge terminal potential of 2.86 V at first cycle, which probably resulted from the presence of the porphyrin-Mn single-site as well. However, the COF-366-Mn discharged down to 2.21 V when cycled to the 30th cycle, indicating an intensified polarization of the battery. On the contrary, TTCOF-Mn and TTCOF-2H cathodes show less potential plateau change compared to that of COF-366-Mn at the 30th cycle. It implies that the role of the electron-donating TTF ligand is essential to the Li-CO_2 performance, especially for cycling tests. Actually, the introduced TTF could indeed improve the conductivity of the COFs.[26−28] As disclosed by the $I-V$ curves in Figure S12, TTCOF-Mn shows a larger slope ($1/R$) value than that of COF-366-Mn, providing solid evidence to the synergistic effect of metalloporphyrin and TTF in enhancing electron transfer. In addition, the Mn 2p XPS spectra of TTCOF-Mn and COF-366-Mn also prove electron migration on the Mn-TAPP site in TTCOF-Mn. As shown in Figure S4, both peaks of Mn $2p_{1/2}$ and Mn $2p_{3/2}$ in the Mn 2p XPS spectrum of TTCOF-Mn shift by ∼0.3 eV to low bonding energy compared with those of COF-366-Mn, which implies a higher electron density of the Mn species given by the electron-donating TTF in TTCOF-Mn.

The Li-CO_2 battery performance was also evaluated at large current densities. Figure S13 shows the discharge−charge curves with different COF cathode catalysts at current densities of 100, 300, and 500 mA/g with a fixed capacity of 1000 mAh/g. The TTCOF-Mn and COF-366-Mn cathode catalysts exhibit high discharge potentials (>2.80 V) at all current densities, which mainly originates from the excellent CO_2 reduction catalytic activity of single-metal porphyrin-Mn sites. In contrast, the TTCOF-2H hardly shows activity toward the Li-CO_2 system, and the discharge terminal potential even drops to 2.12 V at a large current density of 500 mA/g. The voltage gaps between the terminal discharge potential and charge potential, noted as overpotentials, obtained from Figure S13 are given in Figure 2g. The TTCOF-Mn cathodes show overpotentials of 1.07, 1.36, and 1.46 V at 100, 300, and 500 mA/g, respectively. It demonstrates a high activity as a cathode catalyst toward the Li-CO_2 battery, even comparable to the state-of-art cathode catalysts (Table S2). Moreover, the Li-CO_2 battery with TTCOF-Mn cathode could work stably up to 180 cycles with a final discharge terminal potential of 2.60 V at a large current density of 300 mA/g (Figure 2h), whereas

https://dx.doi.org/10.1021/acscentsci.0c01390
ACS Cent. Sci. 2021, 7, 175−182

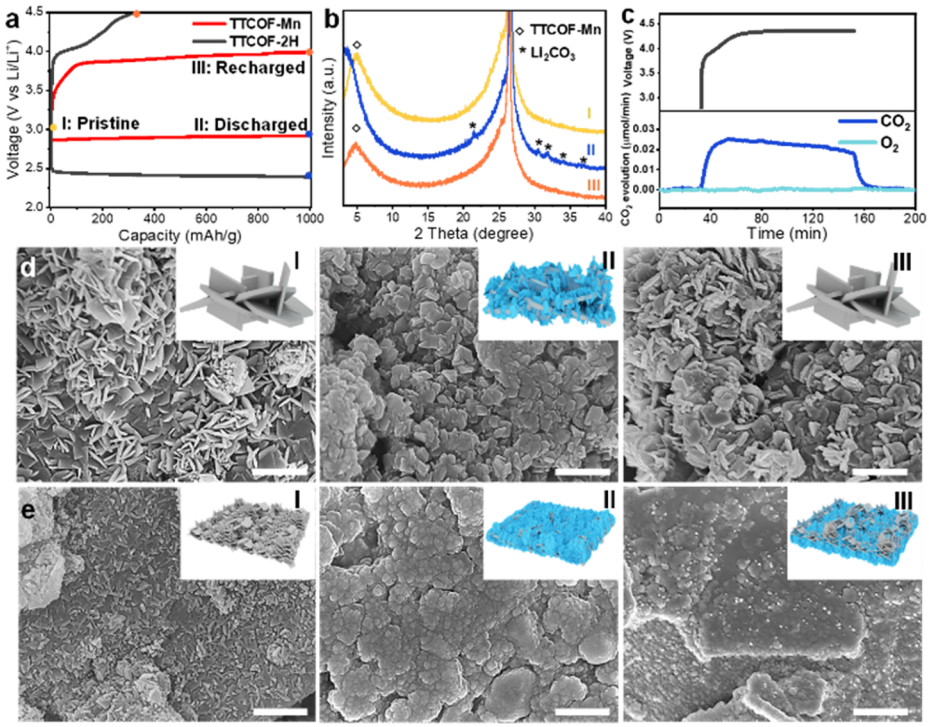

Figure 3. Product characterizations of battery reactions. (a) Discharge−charge curves of TTCOF-Mn and TTCOF-2H cathode catalysts with a fixed capacity of 1000 mAh/g and a voltage range of 2.0−4.5 V vs Li/Li$^+$ with three selected stages of pristine (I), discharge to 1000 mAh/g (II), and recharge back (III). (b) XRD patterns of TTCOF-Mn cathode catalysts at different stages in (a). (c) DEMS test during charging of the Li-CO_2 battery with TTCOF-Mn cathode catalyst. SEM images of (d) TTCOF-Mn cathode catalyst and (e) TTCOF-2H cathode catalyst at different stages in (a), scale bar: 1 μm. The inset in each SEM image represents the schematic illustration of the morphological change of the cathode catalysts.

the battery with the TTCOF-2H cathode could only run for 20 cycles, and the discharge terminal potential decreased quickly down to 1.06 V at the 10th cycle.

The deep discharge−charge profiles of the Li-CO_2 batteries using TTCOF-Mn, TTCOF-2H, and COF-366-Mn as cathode catalysts at 100 mA/g from 2.0 to 5.0 V vs Li/Li$^+$ are presented in Figure S15. It should be noted that all of the batteries are irreversible under the deep discharge state and could not full recharge back after the deep discharging process. The TTCOF-Mn cathode catalyst shows a higher discharge capacity of 13018 mAh/g than that of TTCOF-2H (4192 mAh/g) and COF-366-Mn (8277 mAh/g). Additionally, the Li-CO_2 battery with TTCOF-Mn cathode could recharge back to 10739 mAh/g, showing much better reversibility in contrast to TTCOF-2H and COF-366-Mn.

As the morphology and size of the generated Li_2CO_3 on the cathode surface greatly determine the battery performance, especially during charging, the discharge products at different stages of a discharge−charge cycle with a fixed capacity of 1000 mAh/g were characterized. Three stages of pristine (I), discharge to 1000 mAh/g (II), and recharge back (III) during discharge−charge cycle were selected as shown in Figure 3a. The battery with the TTCOF-2H cathode could not recharge back to 1000 mAh/g within 4.5 V due to the inactive catalysis. As shown from XRD patterns in Figure 3b and Figure S16, the diffraction peak of stage I around 5.1° is assigned to the periodic porosity arrangement of COFs, and the intense peak around 26° belongs to carbon paper. The XRD patterns of stage II in Figure 3b and Figure S16 suggest that the discharge products formed on both TTCOF-Mn and TTCOF-2H cathodes are crystalline Li_2CO_3 (PDF #22-1141). The XRD pattern of stage III in Figure 3b suggests that the Li_2CO_3 on TTCOF-Mn cathode surface has been completely decomposed, and the diffraction peak of TTCOF-Mn emerged again.

SEM images of the TTCOF-Mn and TTCOF-2H cathodes at different stages have been obtained to reveal the state of formed Li_2CO_3. The surface of pristine TTCOF-Mn and TTCOF-2H cathodes is coated by sheet-like COFs with a small amount of particle-like KB (I in Figure 3d,e). The TTCOF-2H sheets are much smaller of than that of TTCOF-Mn. Notably, after discharge, the size of the flake-like Li_2CO_3 formed on TTCOF-Mn cathode is ∼100 nm, much smaller than the Li_2CO_3 particles formed on the TTCOF-2H cathode of 500 nm to 1 μm (II in Figure 3d,e). And the Li_2CO_3 formed on TTCOF-Mn cathode is relatively loose, while the one generated on TTCOF-2H cathode is dense. Then, when recharged, the Li_2CO_3 is incompletely decomposed with a remaining layer on the TTCOF-2H cathode surface (III in Figure 3e). In contrast, almost all of the Li_2CO_3 is decomposed on the TTCOF-Mn cathode (III in Figure 3d), and the COFs maintain the sheet-like morphology, which is consistent with the XRD patterns of stage III in Figure 3b. As shown in Figure S17, the EIS of Li-CO_2 battery with TTCOF-Mn cathode at different stages also confirm the reversibility of the discharge−charge cycle within 1000 mAh/g. After discharging to 1000 mAh/g, the impedance of the battery increased significantly due to the deposition of insulated Li_2CO_3 on the cathode surface. After recharging back, the battery exhibits the interfacial, charge-transfer, and diffusion resistances closed to the pristine state, suggesting most of the discharge products have been decomposed during charging via the CO_2 evolution reaction. Subsequently, the *in situ* differential electrochemical

https://dx.doi.org/10.1021/acscentsci.0c01390
ACS Cent. Sci. 2021, 7, 175−182

mass spectrometry (DEMS) was adopted to monitor the gas evolution of the cell with the TTCOF-Mn cathode during the charging process (Figure 3c). Only CO_2 gas was detected. The charge-to-mass ratio during charging was determined to be $4.17e^-/3CO_2$ according to the result of DEMS, which is close to the theoretical value of $4e^-/3CO_2$ based on the reversible reaction: $4Li^+ + 3CO_2 + 4e^- \rightarrow 2Li_2CO_3 + C$.

To explore the mechanism and reaction pathway of the TTCOF-Mn based Li-CO_2 battery, the discharge product detection of TTCOF-M cathode catalysts together with a series of comprehensive DFT calculations was carried out. The charge/discharge reaction plateaus of TTCOF-M with different metal sites are quite different as shown in Figures S10 and S19−S21. The discharge plateau of TTCOF-Mn remains at ∼2.9 V, and other TTCOF-M (M = Co, Ni, Cu) cathodes show similar discharge plateaus of approximately 2.5 V. It indicates that the reaction pathway of TTCOF-Mn and other TTCOF-M (M = Co, Ni, Cu) are possibly not similar. The discharge gas products of TTCOF-M cathodes (M = Mn, Co, Ni, Cu) were detected by gas chromatography (GC). As shown in Figure S22, obvious signal peaks of CO can be detected in the discharge gas products of TTCOF-Co, TTCOF-Ni, and TTCOF-Cu cathodes, whereas a negligible amount of CO could be found in the discharge gas products of TTCOF-Mn cathodes. Therefore, it could be assumed that the discharge reaction on the TTCOF-Mn cathode might be $4Li + 3CO_2 \rightarrow 2Li_2CO_3 + C$ (E^0 = 2.80 V vs Li/Li^+) with amorphous carbon and crystalline Li_2CO_3 as the main CO_2 reduction products.[13] And on the TTCOF-Co, TTCOF-Ni, and TTCOF-Cu cathode catalysts, it is likely to occur the discharge reaction of $2Li + 2CO_2 \rightarrow Li_2CO_3 + CO$ (E^0 = 2.49 V vs Li/Li^+) with CO and Li_2CO_3 as the main discharge products.[19]

DFT calculations were subsequently conducted to reveal the specific aprotic CO_2 reduction pathways of discharge reactions on different TTCOF-M cathodes. The models for calculation were simplified from TTCOF-M to TAPP-M molecules since the TAPP-M/AC (the mixture of TAPP-M monomer and activated carbon) cathodes performed similarly to the relevant TTCOF-M during the discharge reaction (Figure S23). The adsorption of CO_2 on the active sites of different TAPP-M molecules was simulated at first. As shown in Figure 4a, the distance between the Mn-site in TAPP-Mn and O atom in CO_2 is 2.875 Å and the formation of CO_2@TAPP-Mn shows a free energy of −0.02 eV, suggesting that the adsorption of CO_2 on TAPP-Mn is spontaneous. On the contrary, the adsorption CO_2 on TAPP-Co, TAPP-Ni, and TAPP-Cu is all thermodynamically unfavorable. These results suggested that the TAPP-Mn site exhibits more efficient adsorption ability for CO_2 during the aprotic CO_2 reduction reaction than other three metal sites, which is related to the high activity of the TTCOF-Mn cathode catalyst.

The feasible discharge processes on the TTCOF-Mn cathode were studied by DFT calculations. As the observed discharge plateau of ∼2.9 V is consistent with the calculated thermodynamic potential for the reaction $4Li + 3CO_2 \rightarrow 2Li_2CO_3 + C$ of ∼2.80 V vs Li/Li^+,[30,31] and combining with the results of XRD, DEMS, and GC tests, it could be concluded that the discharge pathway of the TTCOF-Mn cathode catalyst involves a four-electron reduction of CO_2 along with ($Li^+ + e^-$) pairs to form crystalline Li_2CO_3 and a certain form of carbon. The discharge reaction pathway is formed by the sequential reactions including CO_2 adsorption

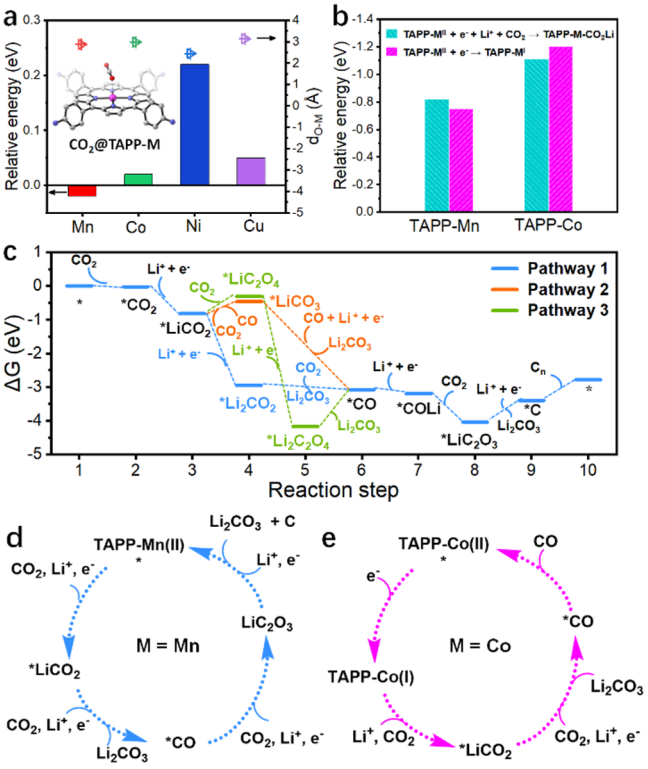

Figure 4. DFT calculations. (a) Energy profiles of CO_2 adsorption on TAPP-M (M = Mn, Co, Ni, Cu) molecules. d_{O-Mn} is the distance between the O atom in CO_2 and the metal atom in TAPP-M. The inset is the corresponding molecular schematic illustration. (b) Energy profiles of the first electron accepted by TAPP-M (M = Mn, Co) molecules in two different pathways. (c) Energetic profiles (ΔG) for Li_2CO_3 nucleation and C_n formation with the three reaction pathways on the TAPP-Mn molecule at U = 0 V. (d) Four-electron pathway occurs on the TAPP-Mn site. (e) Two-electron pathway occurs on the TAPP-Co site.

and reduction of Li^+.[32] The adsorption of CO_2 is set as the first step of the discharge reaction. And the reduction of Li^+ is the second step since the metalloporphyrin site could not react with two CO_2 molecules simultaneously. The possible discharge reaction pathways are listed as Pathway 1−3 in Figure S26. Figure 4c presents the energetic profiles (ΔG) for Li_2CO_3 nucleation and C formation with the three listed reaction pathways on the TAPP-Mn molecule at U = 0 V. Results indicate that Pathway 1 with sequential formation of the intermediate states including $*CO_2$, $*LiCO_2$, $*Li_2CO_2$, *CO, *COLi, $*LiC_2O_3$, and *C is the most energetic favorable among the three possible reaction processes. The calculated discharge reaction pathway demonstrates that efficient CO_2 adsorption, fast Li^+ transfer, and effective electron migration are needed for the high-performance Li-CO_2 battery.

The main possible discharge reaction pathway of other TAPP-M (M = Co, Ni, Cu) cathode catalysts is also revealed. The crucial difference between TAPP-Mn and other TAPP-M (M = Co, Ni, Cu) during the aprotic CO_2 reduction reaction is found to be the first reduction reaction. As shown in Figure 4b and eqs S2−S5, in the TTCOF-Mn system, the first electron tends to react with Li^+ and then combines with a CO_2 molecule to form a TAPP-Mn-CO_2Li intermediate with a ΔG^0 of −0.82 eV (eq S2). On the contrary, the energy for TAPP-Mn(II) itself to be reduced to form TAPP-Mn(I) is −0.75 eV (eq S4). However, as shown in Figure 4b, the first

https://dx.doi.org/10.1021/acscentsci.0c01390
ACS Cent. Sci. 2021, 7, 175−182

electron is likely to reduce the Co(II)-site itself to form a Co(I) catalytic center (eq S5, $\Delta G^0 = -1.20$ eV) rather than Li^+ (eq S3, $\Delta G^0 = -1.11$ eV). In addition, the free energies of TAPP-Ni(II) to form TAPP-Ni(I) and TAPP-Cu(II) to form TAPP-Cu(I) are −1.41 eV (eq S6) and −1.35 eV (eq S7), which are also significantly less negative than that of the Mn-site. As the TAPP-Ni and TAPP-Cu exhibit a similar electrochemical performance and generate the same discharge products as TAPP-Co, it is predictable that the discharge mechanism occurring on the TAPP-Ni site and TAPP-Cu site might be the same as TAPP-Co. Therefore, in contrast with the other TAPP-M (M = Co, Ni, Cu) catalytic sites, the particularity of TAPP-Mn is that it is difficult to be reduced into Mn(I). At the TAPP-Mn catalytic center, the initial electron would participate in a discharge reaction to reduce Li^+ and CO_2, which achieves a four-electron pathway to form Li_2CO_3 and C (Figure 4d). And a two-electron pathway might occur on the TAPP-Co sites with Li_2CO_3 and CO as discharge products (Figure 4e and Figure S27).

■ CONCLUSIONS

In summary, a robust Li-CO_2 battery cathode catalyst was designed based on porphyrin-based covalent organic frameworks (TTCOF-Mn) with uniformly dispersed single-metal sites and unique ordered channels. The TTCOF-Mn cathode exhibits the lowest terminal voltage gap of 1.07 V between discharge and charge potential at 100 mA/g and excellent stability of 180 cycles at 300 mA/g with a fixed 1000 mAh/g capacity, which is among the best Li-CO_2 battery cathode catalysts to date. The active porphyrin-Mn(II) single catalytic sites and fast lithium ion transfer pathways, together with the high electron transfer efficiency, contribute to a high-performance Li-CO_2 system. Density functional theory calculations along with the electrochemical performance reveal that different metalloporphyrin sites lead to different discharge reaction pathways. The single-metal Mn(II) sites in TTCOF-Mn can effectively adsorb the CO_2 molecule and achieve an efficient four-electron aprotic CO_2 conversion route during the discharging−charging process. And the metal site with Co, Ni, or Cu occurs a two-electron pathway to fulfill the discharge reaction. It is the first example to uncover the active catalytical sites and to explore the reaction mechanism from the molecule level in an aprotic Li-CO_2 battery.

■ ASSOCIATED CONTENT

Supporting Information

The Supporting Information is available free of charge at https://pubs.acs.org/doi/10.1021/acscentsci.0c01390.

Detailed information regarding the experimental methods, characterization analysis, and electrochemical measurement (PDF)

■ AUTHOR INFORMATION

Corresponding Author

Ya-Qian Lan − *Jiangsu Collaborative Innovation Centre of Biomedical Functional Materials, Jiangsu Key Laboratory of New Power Batteries, School of Chemistry and Materials Science, Nanjing Normal University, Nanjing 210023, P. R. China; School of Chemistry, South China Normal University, Guangzhou 510006, P. R. China;* orcid.org/0000-0002-2140-7980; Email: yqlan@njnu.edu.cn

Authors

Yu Zhang − *Jiangsu Collaborative Innovation Centre of Biomedical Functional Materials, Jiangsu Key Laboratory of New Power Batteries, School of Chemistry and Materials Science, Nanjing Normal University, Nanjing 210023, P. R. China*

Rong-Lin Zhong − *Laboratory of Theoretical and Computational Chemistry, Institute of Theoretical Chemistry, College of Chemistry, Jilin University, Changchun 130023, P. R. China;* orcid.org/0000-0002-8896-1767

Meng Lu − *Jiangsu Collaborative Innovation Centre of Biomedical Functional Materials, Jiangsu Key Laboratory of New Power Batteries, School of Chemistry and Materials Science, Nanjing Normal University, Nanjing 210023, P. R. China*

Jian-Hui Wang − *Jiangsu Collaborative Innovation Centre of Biomedical Functional Materials, Jiangsu Key Laboratory of New Power Batteries, School of Chemistry and Materials Science, Nanjing Normal University, Nanjing 210023, P. R. China*

Cheng Jiang − *Jiangsu Collaborative Innovation Centre of Biomedical Functional Materials, Jiangsu Key Laboratory of New Power Batteries, School of Chemistry and Materials Science, Nanjing Normal University, Nanjing 210023, P. R. China*

Guang-Kuo Gao − *Jiangsu Collaborative Innovation Centre of Biomedical Functional Materials, Jiangsu Key Laboratory of New Power Batteries, School of Chemistry and Materials Science, Nanjing Normal University, Nanjing 210023, P. R. China*

Long-Zhang Dong − *Jiangsu Collaborative Innovation Centre of Biomedical Functional Materials, Jiangsu Key Laboratory of New Power Batteries, School of Chemistry and Materials Science, Nanjing Normal University, Nanjing 210023, P. R. China;* orcid.org/0000-0002-9276-5101

Yifa Chen − *Jiangsu Collaborative Innovation Centre of Biomedical Functional Materials, Jiangsu Key Laboratory of New Power Batteries, School of Chemistry and Materials Science, Nanjing Normal University, Nanjing 210023, P. R. China;* orcid.org/0000-0002-1718-6871

Shun-Li Li − *Jiangsu Collaborative Innovation Centre of Biomedical Functional Materials, Jiangsu Key Laboratory of New Power Batteries, School of Chemistry and Materials Science, Nanjing Normal University, Nanjing 210023, P. R. China*

Complete contact information is available at: https://pubs.acs.org/10.1021/acscentsci.0c01390

Author Contributions

⊥Y.-Z., R.-L.Z., and M.L. contributed equally to this work.

Notes

The authors declare no competing financial interest.

■ ACKNOWLEDGMENTS

This work was financially supported by NSFC (Nos. 21871141, 21871142, 21701085, and 21901122); the NSF of Jiangsu Province of China (No. BK20171032); the Natural Science Research of Jiangsu Higher Education Institutions of China (Nos. 17KJB150025 and 19KJB150011) and Project funded by China Postdoctoral Science Foundation (Nos. 2018M630572 and 2019M651873); Priority Academic Program Development of Jiangsu Higher Education Institutions

and the Foundation of Jiangsu Collaborative Innovation Center of Biomedical Functional Materials.

■ REFERENCES

(1) Mu, X.; Pan, H.; He, P.; Zhou, H. Li-CO_2 and Na-CO_2 Batteries: Toward Greener and Sustainable Electrical Energy Storage. *Adv. Mater.* **2019**, *32* (27), 1903790.

(2) Xie, J.; Zhou, Z.; Wang, Y. Metal-CO_2 Batteries at the Crossroad to Practical Energy Storage and CO_2 Recycle. *Adv. Funct. Mater.* **2020**, *30* (9), 1908285.

(3) Xie, Z.; Zhang, X.; Zhang, Z.; Zhou, Z. Metal-CO_2 Batteries on the Road: CO_2 from Contamination Gas to Energy Source. *Adv. Mater.* **2017**, *29* (15), 1605891.

(4) Zhang, Z.; Zhang, Q.; Chen, Y.; Bao, J.; Zhou, X.; Xie, Z.; Wei, J.; Zhou, Z. The First Introduction of Graphene to Rechargeable Li-CO_2 Batteries. *Angew. Chem., Int. Ed.* **2015**, *54* (22), 6550−6553.

(5) Qie, L.; Lin, Y.; Connell, J. W.; Xu, J.; Dai, L. Highly Rechargeable Lithium-CO_2 Batteries with a Boron- and Nitrogen-Codoped Holey-Graphene Cathode. *Angew. Chem., Int. Ed.* **2017**, *56* (24), 6970−6974.

(6) Xu, S.; Chen, C.; Kuang, Y.; Song, J.; Gan, W.; Liu, B.; Hitz, E. M.; Connell, J. W.; Lin, Y.; Hu, L. Flexible Lithium-CO_2 Battery with Ultrahigh Capacity and Stable Cycling. *Energy Environ. Sci.* **2018**, *11* (11), 3231−3237.

(7) Zhang, X.; Wang, C.; Li, H.; Wang, X.-G.; Chen, Y.-N.; Xie, Z.; Zhou, Z. High performance Li-CO_2 batteries with NiO-CNT cathodes. *J. Mater. Chem. A* **2018**, *6* (6), 2792−2796.

(8) Ge, B.; Sun, Y.; Guo, J.; Yan, X.; Fernandez, C.; Peng, Q. A Co-Doped MnO2 Catalyst for Li-CO_2 Batteries with Low Overpotential and Ultrahigh Cyclability. *Small* **2019**, *15* (34), 1902220.

(9) Xing, Y.; Yang, Y.; Li, D.; Luo, M.; Chen, N.; Ye, Y.; Qian, J.; Li, L.; Yang, D.; Wu, F.; Chen, R.; Guo, S. Crumpled Ir Nanosheets Fully Covered on Porous Carbon Nanofibers for Long-Life Rechargeable Lithium-CO2 Batteries. *Adv. Mater.* **2018**, *30* (51), 1803124.

(10) Qiao, Y.; Xu, S.; Liu, Y.; Dai, J.; Xie, H.; Yao, Y.; Mu, X.; Chen, C.; Kline, D. J.; Hitz, E. M.; Liu, B.; Song, J.; He, P.; Zachariah, M. R.; Hu, L. Transient, In situ Synthesis of Ultrafine Ruthenium Nanoparticles for a High-rate Li-CO_2 Battery. *Energy Environ. Sci.* **2019**, *12* (3), 1100−1107.

(11) Qiao, Y.; Yi, J.; Wu, S.; Liu, Y.; Yang, S.; He, P.; Zhou, H. Li-CO_2 Electrochemistry: A New Strategy for CO_2 Fixation and Energy Storage. *Joule* **2017**, *1* (2), 359−370.

(12) Yang, S.; Qiao, Y.; He, P.; Liu, Y.; Cheng, Z.; Zhu, J.-J.; Zhou, H. A reversible lithium-CO_2 battery with Ru nanoparticles as a cathode catalyst. *Energy Environ. Sci.* **2017**, *10* (4), 972−978.

(13) Ahmadiparidari, A.; Warburton, R. E.; Majidi, L.; Asadi, M.; Chamaani, A.; Jokisaari, J. R.; Rastegar, S.; Hemmat, Z.; Sayahpour, B.; Assary, R. S.; Narayanan, B.; Abbasi, P.; Redfern, P. C.; Ngo, A.; Voros, M.; Greeley, J.; Klie, R.; Curtiss, L. A.; Salehi-Khojin, A. A Long-Cycle-Life Lithium-CO_2 Battery with Carbon Neutrality. *Adv. Mater.* **2019**, *31* (40), 1902518.

(14) Wei, Y.-S.; Zhang, M.; Zou, R.; Xu, Q. Metal-Organic Framework-Based Catalysts with Single Metal Sites. *Chem. Rev.* **2020**, *120*, 12089.

(15) Rogge, S. M. J.; Bavykina, A.; Hajek, J.; Garcia, H.; Olivos-Suarez, A. I.; Sepulveda-Escribano, A.; Vimont, A.; Clet, G.; Bazin, P.; Kapteijn, F.; Daturi, M.; Ramos-Fernandez, E. V.; Llabres i Xamena, F. X.; Van Speybroeck, V.; Gascon, J. Metal-Organic and Covalent Organic Frameworks as Single-Site Catalysts. *Chem. Soc. Rev.* **2017**, *46* (11), 3134−3184.

(16) Wang, Y.-R.; Huang, Q.; He, C. T.; Chen, Y.; Liu, J.; Shen, F. C.; Lan, Y. Q. Oriented electron transmission in polyoxometalate-metalloporphyrin organic framework for highly selective electroreduction of CO_2. *Nat. Commun.* **2018**, *9* (1), 4466.

(17) Fang, X.; Shang, Q.; Wang, Y.; Jiao, L.; Yao, T.; Li, Y.; Zhang, Q.; Luo, Y.; Jiang, H.-L. Single Pt Atoms Confined into a Metal-Organic Framework for Efficient Photocatalysis. *Adv. Mater.* **2018**, *30* (7), 1705112.

(18) Lu, M.; Liu, J.; Li, Q.; Zhang, M.; Liu, M.; Wang, J.-L.; Yuan, D.-Q.; Lan, Y.-Q. Rational Design of Crystalline Covalent Organic Frameworks for Efficient CO_2 Photoreduction with H_2O. *Angew. Chem., Int. Ed.* **2019**, *58* (36), 12392−12397.

(19) Zhu, H.-J.; Lu, M.; Wang, Y.-R.; Yao, S.-J.; Zhang, M.; Kan, Y.-H.; Liu, J.; Chen, Y.; Li, S.-L.; Lan, Y.-Q. Efficient electron transmission in covalent organic framework nanosheets for highly active electrocatalytic carbon dioxide reduction. *Nat. Commun.* **2020**, *11* (1), 497.

(20) Segura, J. L.; Mancheno, M. J.; Zamora, F. Covalent organic frameworks based on Schiff-base chemistry: synthesis, properties and potential applications. *Chem. Soc. Rev.* **2016**, *45* (20), 5635−5671.

(21) Huang, N.; Wang, P.; Jiang, D. Covalent Organic Frameworks: A Materials Platform for Structural and Functional Designs. *Nat. Rev. Mater.* **2016**, *1* (10), 16068.

(22) Zhu, X.; Tian, C.; Mahurin, S. M.; Chai, S.-H.; Wang, C.; Brown, S.; Veith, G. M.; Luo, H.; Liu, H.; Dai, S. A Superacid-Catalyzed Synthesis of Porous Membranes Based on Triazine Frameworks for CO_2 Separation. *J. Am. Chem. Soc.* **2012**, *134* (25), 10478−10484.

(23) Fu, J.; Das, S.; Xing, G.; Ben, T.; Valtchev, V.; Qiu, S. Fabrication of COF-MOF Composite Membranes and Their Highly Selective Separation of H_2/CO_2. *J. Am. Chem. Soc.* **2016**, *138* (24), 7673−7680.

(24) Huang, N.; Chen, X.; Krishna, R.; Jiang, D. Two-Dimensional Covalent Organic Frameworks for Carbon Dioxide Capture through Channel-Wall Functionalization. *Angew. Chem., Int. Ed.* **2015**, *54* (10), 2986−2990.

(25) Li, X.; Wang, H.; Chen, Z.; Xu, H.-S.; Yu, W.; Liu, C.; Wang, X.; Zhang, K.; Xie, K.; Loh, K. P. Covalent-Organic-Framework-Based Li-CO_2 Batteries. *Adv. Mater.* **2019**, *31* (48), 1905879.

(26) Su, J.; He, W.; Li, X.-M.; Sun, L.; Wang, H.-Y.; Lan, Y.-Q.; Ding, M.; Zuo, J.-L. High Electrical Conductivity in a 2D MOF with Intrinsic Superprotonic Conduction and Interfacial Pseudo-capacitance. *Matter* **2020**, *2* (3), 711−722.

(27) Davis, C. M.; Kawashima, Y.; Ohkubo, K.; Lim, J. M.; Kim, D.; Fukuzumi, S.; Sessler, J. L. Photoinduced Electron Transfer from a Tetrathiafulvalene-Calix 4 pyrrole to a Porphyrin Carboxylate within a Supramolecular Ensemble. *J. Phys. Chem. C* **2014**, *118* (25), 13503−13513.

(28) Jana, A.; Bahring, S.; Ishida, M.; Goeb, S.; Canevet, D.; Salle, M.; Jeppesen, J. O.; Sessler, J. L. Functionalised Tetrathiafulvalene-(TTF-) Macrocycles: Recent Trends in Applied Supramolecular Chemistry. *Chem. Soc. Rev.* **2018**, *47* (15), 5614−5645.

(29) Lin, S.; Diercks, C. S.; Zhang, Y.-B.; Kornienko, N.; Nichols, E. M.; Zhao, Y.; Paris, A. R.; Kim, D.; Yang, P.; Yaghi, O. M.; Chang, C. J. Covalent Organic Frameworks Comprising Cobalt Porphyrins for Catalytic CO_2 Reduction in Water. *Science* **2015**, *349* (6253), 1208−1213.

(30) Xu, S.; Das, S. K.; Archer, L. A. The Li-CO_2 Battery: A Novel Method for CO_2 Capture and Utilization. *RSC Adv.* **2013**, *3* (18), 6656−6660.

(31) Reaction in Li-CO_2 Batteries through Incorporation of CO_2 Capture Chemistry. *Joule* **2018**, *2* (12), 2649−2666.

(32) Yang, C.; Guo, K.; Yuan, D.; Cheng, J.; Wang, B. Unraveling Reaction Mechanisms of Mo_2C as Cathode Catalyst in a Li-CO_2 Battery. *J. Am. Chem. Soc.* **2020**, *142* (15), 6983−6990.